



Simulation of a ridge-type semiconductor laser with transversal diffraction gratings

Tatsuhiro Hirose¹ · Takahiro Numai¹

Received: 15 October 2021 / Accepted: 14 January 2022 / Published online: 9 February 2022
© The Author(s), under exclusive licence to Springer Science+Business Media, LLC, part of Springer Nature 2022

Abstract

This paper reports on improvement of stability of the fundamental horizontal transverse mode in a ridge-type semiconductor laser by incorporating transversal diffraction gratings. Kinks do not appear in current versus light-output curves by appropriately designing the number of the grating periods when the mesa width is $5\ \mu\text{m}$ in which kinks exist in current versus light-output curves for conventional ridge-type semiconductor lasers.

Keywords Semiconductor laser · Diffraction grating · Horizontal transverse mode

1 Introduction

Due to COVID-19 people are obliged to work from home and join online meetings. As a result, capacity of telecommunications has been running short. To overcome this problem, capacity and E/O conversion efficiency of trunk lines of telecommunications have to be improved.

As trunk lines, long-span optical fibers with Er^{3+} -doped optical fiber amplifiers (EDFAs) have been used. To pump EDFAs, high power 980-nm semiconductor lasers (Harder et al. 1997) have been utilized. In general, the high power 980-nm semiconductor lasers have ridge structures to confine horizontal transverse modes. The reason why ridge structures are adopted in the high power 980-nm semiconductor lasers are as follows: the high power 980-nm semiconductor lasers have $\text{In}_{0.2}\text{Ga}_{0.8}\text{As}$ active layers and AlGaAs cladding and guiding layers. The AlGaAs layers are oxidized easily during etching processes and the oxidized AlGaAs layers highly degrade electrical and optical characteristics of the high power 980-nm semiconductor lasers. To avoid these problems, ridge structures are adopted.

This article is part of the Topical Collection on Numerical Simulation of Optoelectronic Devices.

Guest edited by Slawek Sujecki, Asghar Asgari, Donati Silvano, Karin Hinzer, Weida Hu, Piotr Martyniuk, Alex Walker and Pengyan Wen.

✉ Takahiro Numai
numai@se.ritsumeikai.ac.jp

¹ College of Science and Engineering, Ritsumeikan University, 1-1-1 Noji-Higashi, Kusatsu, Shiga 525-8577, Japan

In the ridge structures, higher-order horizontal transverse modes as well as the fundamental horizontal transverse mode are confined to their waveguides. Therefore, with an increase in injected current, higher-order horizontal transverse modes lase; kinks appear in their current versus light-output (I - L) curves (Schemmann et al. 1995). Below the kink level — the light-output where a kink appears in I - L curve — only the fundamental horizontal transverse mode oscillates; above the kink level, higher-order horizontal transverse modes oscillate. The higher-order horizontal transverse modes have much lower light coupling efficiency to the single mode optical fibers than the fundamental horizontal transverse mode, which leads to low E/O conversion efficiency.

To achieve high light coupling efficiency between the high power 980-nm semiconductor lasers and the single mode Er^{3+} -doped optical fibers, high kink level or kink-free operation of the high power 980-nm semiconductor lasers is needed. To increase the kink level in the ridge structures, lossy metal layers (Buda et al. 2003), highly resistive regions in both sides of the ridge stripe (Yuda et al. 1998), incorporation of a graded V-shape layer (Qiu et al. 2005), optical antiguiding layers (Shomura et al. 2008; Yoshida and Numai 2009), separate confinement of carriers and horizontal transverse mode (Kato et al. 2013), and horizontal coupling of horizontal transverse modes by a groove in the mesa (Chai and Numai 2014) have been studied.

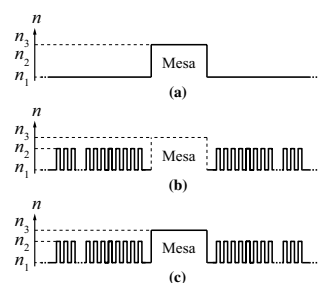
In this paper, a ridge-type semiconductor laser with transversal diffraction gratings is proposed to obtain kink-free operation. From simulations, it is found that kink-free operation is obtained by appropriately designing the number of the grating periods.

2 Operating principle

Figure 1 shows operating principles for confining laser light in the waveguide by index guiding. The vertical line shows the refractive index; the horizontal line is normal to both of the cavity axis and the direction of the epitaxial growth; parallel to facets of a 980-nm semiconductor laser. In Fig. 1, (a) illustrates the distribution of the refractive index of a conventional ridge structure, (b) draws the distribution of the refractive index of transversal diffraction gratings, and (c) reveals a coupled distribution of the refractive index of the ridge structure and the transversal diffraction gratings.

Both of the ridge structure and the diffraction gratings make the light waves resonate; the transversely resonant modes confined in the waveguide propagates along the cavity axis. In general the wavelengths of the resonant modes of the ridge structure are different from the wavelengths of the resonant modes of the diffraction gratings. We design the waveguide so that the wavelength of the fundamental horizontal transverse mode of the

Fig. 1 Operating principle: **a** ridge, **b** transversal diffraction gratings, **c** coupled



ridge structure and that of the diffraction gratings may agree with each other. As a result, only the fundamental horizontal transverse mode is confined to the waveguide with optical gain. The wavelength difference between the fundamental horizontal transverse mode and the higher-order horizontal transverse modes generated by the diffraction gratings are much smaller than that by the ridge structure. Since the near field patterns (NFPs) of the horizontal transverse modes are obtained by Fourier transform of the optical spectra, small wavelength difference between the resonant modes leads to a large difference in the peak positions of the NFPs for the resonant modes. Therefore, the higher-order horizontal transverse modes are located in a region with optical loss while the fundamental horizontal transverse mode exists in a region with optical gain.

Effect of the diffraction grating is characterized by the grating coupling coefficient κ and the grating region length L . For the rectangular diffraction grating, the grating coupling coefficient κ is given by

$$\kappa = \frac{2(n_2 - n_1)}{\lambda_0} \cdot \frac{\sin(\pi m \gamma)}{m} \quad (1)$$

where λ_0 is the Bragg wavelength which is the wavelength of the laser light, m is the order of the diffraction grating, and γ is the duty ratio of the diffraction grating. In this paper, γ is 1/2. The grating region length L is written as

$$L = 2N\Lambda = 2Nm\Lambda_0 \quad (2)$$

where N is the number of the periods at one side of the mesa, Λ is the grating pitch, and Λ_0 is the grating pitch for the grating with $m = 1$. We denote an NFP by $f(x)$ where x shows a horizontal position and denote a transmission spectrum for the diffraction grating by $F(k)$ where k is a wave number of the horizontal transverse mode. When κ is smaller and L is larger, differences between the k value for the fundamental horizontal transverse mode and the k values for the higher order horizontal transverse modes are smaller, leading to larger differences between the peak position of the fundamental horizontal transverse mode and the peak positions of the higher order horizontal transverse modes. When only the fundamental horizontal transverse mode exists in the optical gain region and the higher order horizontal transverse modes are placed in the optical loss region, we obtain stable single transverse mode operation. In order to obtain a small κ value, $(n_2 - n_1)$ should be small and m should be large from Eq. (1). In order to obtain a large L value, N and m should be large from Eq. (2). As a result, we use $m = 3$ in spite of $m = 1$ in this paper.

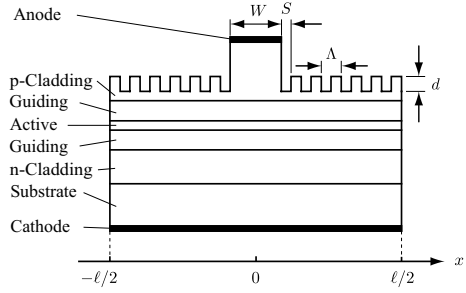
It should be noted that the transversal diffraction gratings are used in the total reflection condition; the diffraction gratings in DFB or DBR semiconductor lasers are used in the condition far from the total reflection condition.

The propagation constant of the waveguide and the light field distribution are obtained by solving an eigenvalue equation for multi-layer optical waveguide (Numai 2015).

3 Structure and simulation model

Figure 2 shows a schematic cross-sectional view of the facet of the proposed ridge structure with transversal diffraction gratings. By utilizing the difference between the spatial distribution of the fundamental horizontal transverse mode and those of higher-order horizontal transverse modes generated by the transversal diffraction gratings, only the fundamental horizontal transverse mode is confined in the optical gain region; the higher-order

Fig. 2 Schematic cross-sectional view of the facet of the proposed ridge structure with transversal diffraction gratings



horizontal transverse modes are located in the optical loss region. In Fig. 2, W is the mesa width, S is the space between the mesa and the diffraction gratings, Λ is the grating pitch, and d is the grating depth. In this paper, we use $W = 5.0 \mu\text{m}$, $S = 426 \text{ nm}$, $\Lambda = 428.7 \text{ nm}$, and $d = 400 \text{ nm}$. Note that $W = 5.0 \mu\text{m}$ leads to kink in I - L curves for conventional ridge-type semiconductor lasers. The height of the mesa is $1.55 \mu\text{m}$ and width of the base l is $60 \mu\text{m}$. The origin of the x -axis is located at the center of the mesa; the x -axis is normal to both of the cavity axis and the direction of the epitaxial growth. The cavity length is $1200 \mu\text{m}$. Power reflectivities of the front and rear facets are 2 and 90%, respectively.

Layer parameters which are summarized in Table 1 are the same as those described in Refs. Shomura (2008), Yoshida (2009), Kato (2013), Chai and Numai (2014). Lasing characteristics are simulated by using a device simulation software ATLAS (Silvaco) in which Poisson's equations and Helmholtz equation are solved with a finite element method. To determine the transverse optical field, a two-dimensional Helmholtz equation is solved. ATLAS has four optical gain models and the optical gain spectrum in this paper is obtained from the spontaneous emission spectrum (Lim et al. 2007). The optical gain depends on the quasi-Fermi levels and in turn impacts dielectric permittivity. Spontaneous recombination and non-linear gain saturation (Boyd 1992) are also calculated.

4 Simulated results and discussions

Figure 3 shows injected current versus applied voltage (I - V) curves. The parameter is the number of the grating periods N at one side of the mesa. The broken line shows the result for $N = 20$, and the solid line shows the results for $N \geq 25$. Note that the I - V curves for $N \geq 25$ are overlapped. A differential resistance for $25 \leq N \leq 50$ is lower than that for $N = 20$, because the transversal diffraction gratings contribute to confinement of the carriers below the mesa.

Fig. 3 Current versus voltage curve

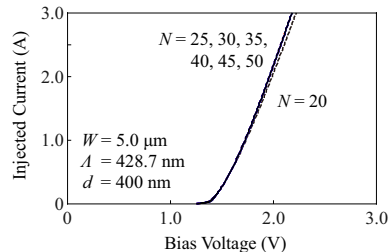


Fig. 4 Current versus light-output curve

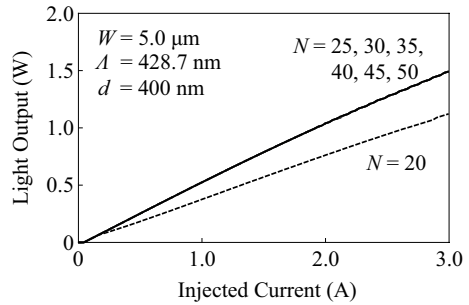


Fig. 5 Distribution of electron concentration

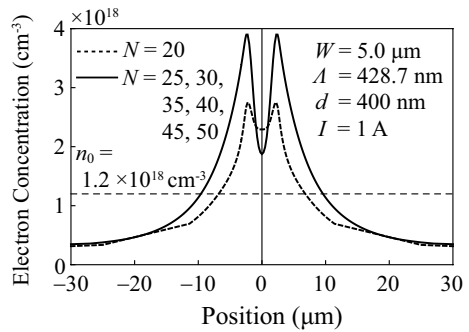


Figure 4 shows injected current versus light-output (I - L) curves. The parameter is the number of the grating periods N at one side of the mesa. The broken line shows the result for $N = 20$, and the solid line shows the results for $25 \leq N \leq 50$. Note that the curves for $25 \leq N \leq 50$ are overlapped. When $N = 20$, a kink appears in I - L curve with oscillation of the first-order horizontal transverse mode. When $N \geq 25$, kinks do not exist in I - L curves and only the fundamental horizontal transverse mode oscillates up to the injected current of 3 A.

Figure 5 shows the distribution of the electron concentration for the injected current $I = 1$ A. The vertical line shows the electron concentration; the horizontal line is x -axis in Fig. 2. The parameter is the number of the grating periods N at one side of the mesa. The transparent carrier concentration n_0 where the optical gain is 0 cm^{-1} is $1.2 \times 10^{18} \text{ cm}^{-3}$.

The broken line shows the result for $N = 20$, and the solid line shows the results for $25 \leq N \leq 50$. Note that the curves for $25 \leq N \leq 50$ are overlapped. The electron concentration in the origin of the horizontal axis — the center of the mesa — is lower than those in the both sides, because of the spatial hole burning. At the center of the mesa the electron concentration for $25 \leq N \leq 50$ is lower than that for $N = 20$, because the electron consumption due to stimulated emission with single transverse mode operation for $25 \leq N \leq 50$ is larger than that for $N = 20$ with two-mode operation.

Figure 6 shows NFPs for the fundamental horizontal transverse modes for the injected current $I = 1$ A. The parameter is the number of the grating periods N at one side of the mesa. The broken line shows the result for $N = 20$, and the solid line shows the results for $25 \leq N \leq 50$. Note that the curves for $25 \leq N \leq 50$ are overlapped. Kink appears in I - L curve when $N = 20$; kink does not exist in I - L curve when $25 \leq N \leq 50$. The NFPs almost overlapped with FWHM = $3.0 \mu\text{m}$, irrespective of existence or non-existence of kink.

Fig. 6 Near field patterns for the fundamental horizontal transverse modes

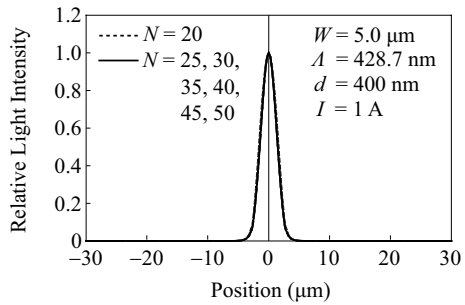


Figure 7 shows the NFPs for the first-order horizontal transverse modes for $I = 1$ A. The vertical line shows relative light intensity where a maximum of each curve is set to unity; the horizontal line shows x -axis in Fig. 2. The parameter is the number of the grating periods N at one side of the mesa, and N changes from 20 to 50 in steps of 5. The broken line shows the result for $N = 20$, the thick solid line for $N = 25$, the dotted line for $N = 30$, the thin solid line for $N = 35$, the dash-dotted line for $N = 40$, the dashed line for $N = 45$, and the dash-double-dotted line for $N = 50$. When $N = 20, 25$, and 30 , each NFP has two peaks which are symmetric with respect to the vertical axis. When $N = 35$, the NFP has a single peak in $x < 0$. When $N = 40, 45$, and 50 , each NFP has two peaks which are asymmetric with respect to the vertical axis; each peak in $x < 0$ is larger than that in $x > 0$. With an increase in N , that is, with an increase in L , distances between the the peak position of the fundamental horizontal transverse mode — the origin of the horizontal axis — and the peak positions of the higher order horizontal transverse modes increase. Since the optical cavity along the horizontal axis is a coupled cavity of the ridge structure and the diffraction gratings, the NFPs show complicated behaviors according to the values of N .

When $N = 20$ the NFP for the first-order horizontal transverse mode exists in the optical gain region where $n > n_0 = 1.2 \times 10^{18} \text{ cm}^{-3}$, leading to kink in I - L curve. When $N = 25$ the NFP exists in the optical loss region where $n < n_0 = 1.2 \times 10^{18} \text{ cm}^{-3}$, leading to kink-free operation.

Figure 8 shows threshold current I_{th} for the fundamental horizontal transverse mode as a function of the grating periods N at one side of the mesa. Threshold current has the lowest value at $N = 40$. As explained earlier, the first-order horizontal transverse mode does not oscillate when $N \geq 25$. Therefore the NFP of the first-order horizontal transverse mode in $N \geq 25$ is not considered to affect the threshold current of the fundamental horizontal transverse mode.

Fig. 7 Near field patterns for the first-order horizontal transverse modes

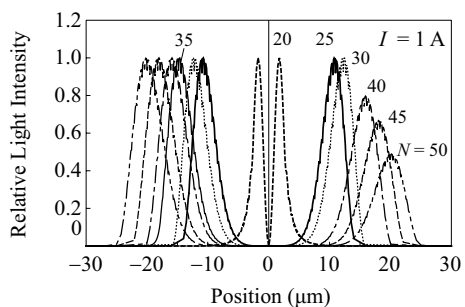
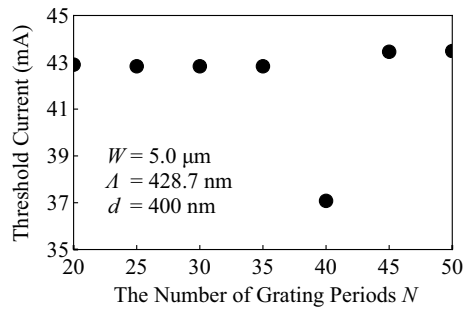


Fig. 8 Threshold current for the fundamental horizontal transverse mode versus the number of the grating periods at one side



We consider threshold current from the viewpoint of overlapping of the optical field and the electron concentration in the following. We define the convolution h of the light distribution and the electron distribution as

$$h = \int_{-\ell/2}^{\ell/2} I(x)n(x) dx \quad (3)$$

where x -axis is the horizontal axis shown in Fig. 5, ℓ is width of the base, $I(x)$ is normalized light intensity, and $n(x)$ is the electron concentration in the active layer.

Figure 9 shows the convolution h of the light distribution and the electron distribution for the fundamental horizontal transverse mode for the injected current $I = 40$ mA ($< I_{th}$). The convolution h has the highest value at $N = 40$, leading to the lowest I_{th} as shown in Fig. 8.

Figure 10 shows the convolution h of the light distribution and the electron distribution for the first-order horizontal transverse mode for $I = 1$ A. The convolution h has the highest value at $N = 20$, leading to kink in I - L curve; the convolution h for $25 \leq N \leq 50$ is lower than that for $N = 20$.

5 Summary

To improve kink levels, a ridge-type semiconductor laser with transversal diffraction gratings was proposed and simulated. It is found that kinks do not appear by designing the number of the grating periods appropriately when the mesa width is as wide as $5 \mu\text{m}$.

Fig. 9 Convolution of the light distribution and the electron distribution for the fundamental horizontal transverse mode

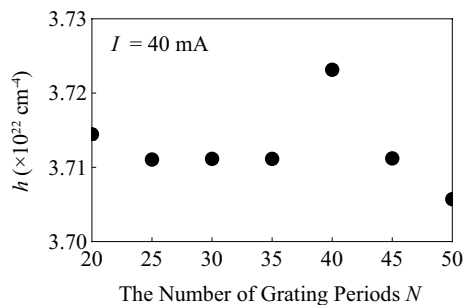


Fig. 10 Convolution of the light distribution and the electron distribution for the first-order horizontal transverse mode

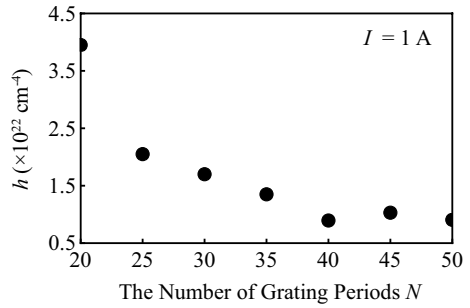


Table 1 Layer parameters

Layer	Band gap energy (eV)	Refractive index
p-Al _{0.2} Ga _{0.8} As Cladding	1.721	3.424
Al _{0.15} Ga _{0.85} As Guiding	1.650	3.453
Al _{0.1} Ga _{0.9} As Barrier	1.583	3.482
In _{0.2} Ga _{0.8} As QW Active	1.260	3.650
Al _{0.03} Ga _{0.97} As Barrier	1.474	3.520
n-Al _{0.2} Ga _{0.8} As Cladding	1.721	3.424
n-GaAs Substrate	1.424	3.540
Layer	Thickness (μm)	Doping concentration (cm^{-3})
p-Al _{0.2} Ga _{0.8} As Cladding	1.6	8×10^{17}
Al _{0.15} Ga _{0.85} As Guiding	0.2	undoped
Al _{0.1} Ga _{0.9} As Barrier	0.01	undoped
In _{0.2} Ga _{0.8} As QW Active	0.01	undoped
Al _{0.03} Ga _{0.97} As Barrier	0.01	undoped
n-Al _{0.2} Ga _{0.8} As Cladding	1.5	1×10^{18}
n-GaAs Substrate	100	2×10^{18}
Layer	Electron effective mass	Hole effective mass
p-Al _{0.2} Ga _{0.8} As Cladding	$0.0834m_0$	$0.6738m_0$
Al _{0.15} Ga _{0.85} As Guiding	$0.0793m_0$	$0.6657m_0$
Al _{0.1} Ga _{0.9} As Barrier	$0.0753m_0$	$0.6464m_0$
In _{0.2} Ga _{0.8} As QW Active	$0.0622m_0$	$m_{\text{hh}}(xy) = 0.1238m_0$ $m_{\text{hh}}(z) = 0.5885m_0$ $m_{\text{lh}}(xy) = 0.0938m_0$ $m_{\text{lh}}(z) = 0.0587m_0$
Al _{0.03} Ga _{0.97} As Barrier	$0.0695m_0$	$0.6415m_0$
n-Al _{0.2} Ga _{0.8} As Cladding	$0.0834m_0$	$0.6738m_0$
n-GaAs Substrate	$0.0630m_0$	$0.5700m_0$

$m_0 = \text{Electron Rest Mass}$

References

- Boyd, R.W.: *Nonlinear Optics*. Academic Press, New York (1992)
- Buda, M., Tan, H.H., Fu, L., Josyula, L., Jagadish, C.: Improvement of the kink-free operation in ridge-waveguide laser diodes due to coupling of the optical field to the metal layers outside the ridge. *IEEE Photon. Technol. Lett.* **15**, 1686–1688 (2003)
- Chai, G., Numai, T.: Simulation of a ridge-type semiconductor laser with horizontal coupling of lateral modes. *Opt. Quantum Electron.* **46**, 1217–1223 (2014)
- Harder, C. S., Brovelli, L., Meier, H. P., and Oosenbrug, A.: High reliability 980-nm pump lasers for Er amplifiers, *Proc. Optical Fiber Communication Conf. '97*, Dallas, USA, 350 (1997)
- Kato, H., Yoshida, H., Numai, T.: Simulation of a ridge-type semiconductor laser for separate confinement of horizontal transverse modes and carriers. *Opt. Quantum Electron.* **45**, 573–579 (2013)
- Lim, J.J., MacKenzie, R., Sujecki, S., Sadeghi, M., Wang, S.M., Wei, Y.Q., Gustavsson, J.S., Larsson, A., Melanen, P., Sipilä, P., Uusimaa, P., George, A.A., Smowton, P.M., Larkins, E.C.: Simulation of double quantum well GaInNAs laser diodes. *IET Optoelectron.* **1**, 259–265 (2007)
- Numai, T.: *Fundamentals of semiconductor lasers*, Second edition, pp.58–62, Springer, Tokyo, 2015
- Qiu, B., McDougall, S.D., Liu, X., Bacchin, G., Marsh, J.H.: Design and fabrication of low beam divergence and high kink-free power lasers. *IEEE J. Quantum Electron.* **41**, 1124–1130 (2005)
- Schemmann, M.F.C., van der Poel, C.J., van Bakel, B.A.H., Ambrosius, H.P.M.M., Valster, A., van den Heijkant, J.A.M., Acket, G.A.: Kink power in weakly index guided semiconductor lasers. *Appl. Phys. Lett.* **66**, 920–922 (1995)
- Shomura, N., Fujimoto, M., Numai, T.: Fiber pump semiconductor lasers with optical antiguiding layers for horizontal transverse modes. *IEEE J. Quantum Electron.* **44**, 819–825 (2008)
- Yoshida, H. and Numai, T.: Ridge-type semiconductor lasers with antiguiding layers for horizontal transverse modes: dependence on space in the antiguiding layers, *Jpn. J. Appl. Phys.* **48**: 082105-1-5 (2009)
- Yuda, M., Hirono, T., Kozen, A., Amano, C.: Improvement of kink-free output power by using highly resistive regions in both sides of the ridge stripe for 980-nm laser diodes. *IEEE J. Quantum Electron.* **40**, 1203–1207 (1998)

Publisher's Note Springer Nature remains neutral with regard to jurisdictional claims in published maps and institutional affiliations.